



Modeling and generation of electrodynamic modes of a self-sustaining active sensor with Josephson junction

N. G. Koudafoké² · C. H. Miwadinou^{1,2} · A. V. Monwanou² · A. L. Hinvi^{2,3} · J. B. Chabi Orou²

Received: 13 February 2019 / Revised: 1 November 2019 / Accepted: 4 November 2019
© Springer-Verlag GmbH Germany, part of Springer Nature 2019

Abstract

This work deals with the modeling of an active sensor consisting of a Josephson junction, a micro-beam immersed in a uniform magnetic field B , a dipole (r, L, C) and an auxiliary generator. In this work, an active sensor (independent of an external energy supply) capable of converting low temperature and/or a uniform magnetic field B into sinusoidal electrical voltage has been constructed. Being known as an excellent voltage-frequency converter, we have in a second time studied the influence of the Josephson junction on the oscillation frequency of the electrical and mechanical parts of the Micro Electro-Mechanical System. An analytical study of the fixed points and their stability is done. On the other hand, the numerical studies have been done in order to show how the energy losses are compensated thanks to a simple rheostat of the auxiliary generator. The order of the influence of the Josephson junction on the oscillation frequencies and the different electrodynamic modes has been obtained.

Keywords Modelization · Josephson junction · Active sensor · Stability · Micro-electromechanical system · Periodic and chaotic vibrations

1 Introduction

From aeronautics to meteorology and in almost all scientific fields, MEMS/NEMS, and sensors/actuators have become indispensable tools for the practicability and efficiency of the latest generation of devices. Michael Roukes in his article “Nanoelectromechanical systems face the future” has strongly demonstrated what is an electromechanical system, the contributions of nanomachines, the procedure of their manufacture, the challenge of NEMS and some of their interesting applications [1]. In other works, Roukes, Ekinci, Etaki, Bullard, Matheny, Cross, Karabalin and many other researchers have studied the thermal, electrical and mechanical behaviors of micro/nanobeams and nanotubes. The formulas giving the quantities like the total and effective mass, the own frequency, the kinetic energy, the fluctuation

of the temperature of the micro/nano-beam, the amplitude of vibration, the constant of stiffness, the own pulsation, the intrinsic damping coefficient of the micro/nano-beam, the speed of a point along the micro/nano-beam and many other important parameters such as the quality factor Q , micro/nano-beams are well defined. In many fields such as industry, engineering, scientific research, services, hobbies ..., the need to control the physical parameters such as the temperature, the forces, the pressure, the speed, the luminosity ... are inevitably felt. The sensor proves to be an essential element for the detection of these physical quantities. Indeed, a sensor is an organ (passive or active) information gathering which develops from a measurable physical size, another usable physical quantity of different nature (often electrical). This magnitude representative of the sampled quantity can be used for measurement or control purposes. We distinguish several types of sensors generally classified in two major categories: passive sensors and active sensors. Our work here focuses on the latter category (active sensor) given its characteristics and abilities in many scientific fields. Indeed, an active sensor operates as a generator and is generally based in principle on the physical effect that ensures the conversion into electrical energy from the form of energy associate

✉ C. H. Miwadinou
clement.miwadinou@imsp-uac.org

¹ École Normale Supérieure de Natitingou, Natitingou, Benin

² Institut de Mathématiques et de Sciences Physiques, Dangbo, Bénin

³ Institut National des Sciences et Techniques Industrielles, Lokossa, Bénin

to the greatness physical to take. The physical effects most often encountered in instrumentation are:

- The thermo-electric effect: a circuit formed of two conductors of different chemical nature, including junctions are at different temperatures T_1 and T_2 , is the seat of an electromotive force of thermal origin $e(T_1, T_2)$.
- The piezoelectric effect: following the application of a mechanical stress to certain so-called piezoelectric materials (quartz for example), we note the appearance of an electric charge proportional to the deformation undergone and of different sign on opposite sides.
- The photoelectric effect: the release of electric charges into the material under the influence of a light radiation or more generally of an electromagnetic wave.
- The photovoltaic effect: the modification of the voltage at the terminals of an illuminated PN junction following the displacement of the holes and electrons released in the vicinity of the latter.
- The magnetic induction effect: the variation of the magnetic induction flux in an electric circuit induces a voltage.
- Hall effect: a magnetic field B and a current i create in the material a potential difference U_H .

The limited number of these physical effects serving in the construction of these types of sensors make them the least numerous models but the most used because of their ability to serve in many areas.

The active sensor that we propose in this work uses simultaneously the last two physical effects mentioned above namely: the magnetic induction effect and the Hall effect. Indeed the coil of the dipole (r_0, L_0, C_0) is crossed by a variable current i_p . The magnetic flux through this coil is such that $\Phi = L_0 \cdot i_p$. Any variation of the current i_p causes that of Φ which then induces an electric voltage e such that $e = -L_0 \frac{di_p}{dt}$ (Magnetic induction effect). Under the effect of the magnetic field and traversed by the current i_p , is created in the vibrating membrane of the micro-beam a difference potential e_p as defined below (Hall Effect). All these potential differences thus generated are reinjected into the circuit and contribute to the burden of capacitor C_0 (Fig. 1). Amplitudes of oscillations of electro-mechanical system will be controlled by a rheostat of the auxiliary generator and the controlled frequencies by the voltage-frequency converter that is the Josephson junction. The interremain of this junction is due to its interremaining features and dynamic modes that it can generate. Indeed, the Josephson effect since its prediction in 1962 by Brian Josephson has been the subject of an exhaustive list of scientific research. The dynamic behaviors and interremaining features of the Josephson junction have been studied [2–8]. Recently, the dynamics of three and four

non-identical Josephson junctions connected in series and coupled with an RLC dipole are studied [9]. Our motivations for this study are also justified by the recently research on the electromechanical systems. For example, the electromechanical coupling to obtain a MEMS was done by Domguia et al. [10] where electrodynamic equations, stability analysis and dynamic behaviors were studied for a MEMS consisting of a micro-beam coupled to an Hindmarsh–Rose electric oscillator. Yamapi et al. [11] studied the harmonic dynamics and transition to chaos in a nonlinear electromechanical system with parametric coupling. They shown that the dynamics of their electromechanical system can be described by an electrical Duffing oscillator coupled gyroscopically and parametrically to a linear mechanical oscillator. Also, Yamapi and Filatrella [12] studied the noise effect on birhythmic Josephson junction coupled to a resonator. They have found that the stability analysis of Josephson junction coupled to a resonator shows a striking change in the birhythmic region. The attractor characterized by a frequency locked to the resonator is most stable for low bias current, when the power dissipated in the cavity is small. Inspired by all this literature, we propose to model and generate the dynamic modes of an active sensor whose energy losses are compensated by an auxiliary generator and whose oscillation frequencies are controlled by a Josephson junction.

In Sect. 2, we establish the electrodynamic equations of the electric part and of the mechanic part using the Euler–Bernoulli theories which gives the general equation of flexural vibration of the beams [10,13]. Section 3, studies the fixed points and their stabilities using the Routh criteria technique [14]. Considering that depending on the field of study, it is sometimes useful or undesirable to the point where many researchers are interremained in the prediction of chaos and/or its control [15–20], we evaluated and controlled some chaotic dynamics of the sensor in Sect. 4. These etaps will allow us to analyze the influence of each control parameter in general and of Josephson junctions in particular on the oscillatory dynamics of the actif sensor. We provided a conclusion in the last section.

2 Presentation and modelization of the MEMS

The MEMS (Fig. 1) that we propose to study is an auxiliary generator, a Josephson junction and a micro-beam in series with an oscillator (r, L, C). The objective of this study is to build a quasi-self-sufficient MEMS energetically. Indeed, the electric energy of the Joule dipole dissipated by the Joule effect in the electromechanical system at the ohmic conductors will be partially offset by the energy supply of an auxiliary generator. The operational amplifier is supposed to be ideal. We have

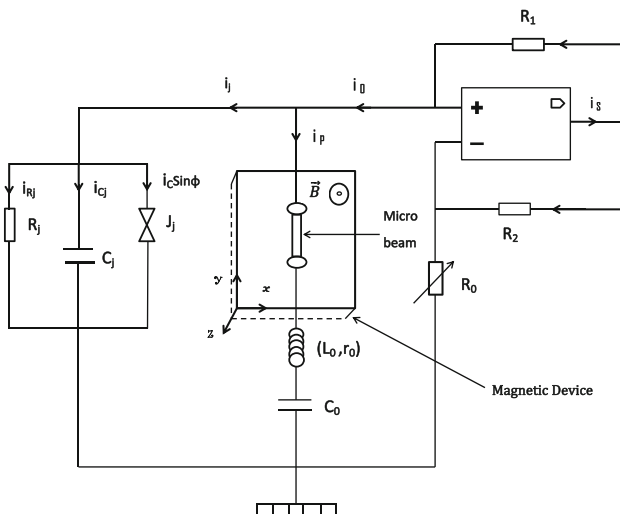


Fig. 1 Device of the self-maintained MEMS where the Josephson junction is represented by its RCSJ model

$$i^+ = i^- = 0 \quad \text{and} \quad \varepsilon = V_e^+ - V_e^- = 0$$

Let's put the auxiliary generator voltage U_g and the potential V_s at the output point of the Operational Amplifier (AO). By applying the Kirchhoff law for the loop voltage, we obtain

$$U_g = R_0 \cdot i_2 + \varepsilon,$$

with

$$i_2 = \frac{R_1 \cdot i_0}{R_2}.$$

Thus,

$$U_g = \frac{R_0 \cdot R_1}{R_2} \cdot i_0 = K \cdot i_0.$$

2.1 Equation of electrical part

Using the current law, we have

$$i_0 = i_p + i_j, \quad (1)$$

$$i_0 = \frac{\hbar}{2eR_j} \frac{d\varphi}{dt} + \frac{\hbar C_j}{2e} \frac{d^2\varphi}{dt^2} + I_c \sin \varphi + i_p. \quad (2)$$

On the other hand,

$$i_p = \frac{dq}{dt} + \frac{e}{r_p} \quad \text{with} \quad \frac{e_p}{r_p} = \frac{-2BA}{\mu L} \int_0^L \frac{\partial u(z, t)}{\partial t} dz.$$

Thus,

$$i_0 = \frac{\hbar}{2eR_j} \frac{d\varphi}{dt} + \frac{\hbar C_j}{2e} \frac{d^2\varphi}{dt^2} + I_c \sin \varphi + \frac{dq}{dt} + \frac{e}{r_p}.$$

Furthermore, $i_0 = \frac{u_g}{K} = \frac{\hbar}{2eK} \dot{\varphi}$. We then obtain

$$\frac{\hbar C_j}{2e} \frac{d^2\varphi}{dt^2} + \frac{\hbar}{2e} \left(\frac{K - R_j}{R_j K} \right) \frac{d\varphi}{dt} + I_c \sin \varphi + \frac{dq}{dt} - \frac{2BA}{\mu L} \int_0^L \frac{\partial u(z, t)}{\partial t} dz = 0. \quad (3)$$

Next, the differential equation that governs the charge q of the capacitor in the circuit is determined. Indeed,

$$u_g = u_p + u_{L_0} + u_{C_0} \quad (4)$$

and

$$K(i_p + i_j) = (r_p \cdot i_p - e_p) + \left(r_0 \cdot i_p + L_0 \frac{di_p}{dt} \right) + \frac{q}{c}. \quad (5)$$

Replacing i_p , $\frac{e_p}{r_p}$, $\frac{di_p}{dt}$ by their expressions into Eq. (5), one obtains:

$$\begin{aligned} \ddot{q} + \left(\frac{r_p + r_0 - K}{L_0} \right) \dot{q} + \frac{1}{L_0 C_0} q - \frac{K I_c}{L_0} \sin \varphi(t) \\ - \left(\frac{r_p + r_0 - K}{L_0} \right) \frac{2BA}{\mu L} \int_0^L \frac{\partial u(z, t)}{\partial t} dz \\ + \frac{2B}{L_0} \int_0^L \frac{\partial u(z, t)}{\partial t} dz - \frac{2BA}{\mu L} \int_0^L \frac{\partial^2 u(z, t)}{\partial t^2} dz \\ - \frac{K \hbar C_j}{2e L_0} \ddot{\varphi}(t) - \frac{K \hbar}{2e L_0 C_j} \dot{\varphi}(t) = 0. \end{aligned} \quad (6)$$

It can be seen that the coefficient of the dissipative term of the load depends on K and can be canceled for a value of R_0 . For this, setting $r_p + r_0 - K = \Delta_r$ and $\omega_0^2 = \frac{1}{L_0 C_0}$, we obtain

$$\begin{aligned} \ddot{q} + \frac{\Delta_r}{L_0} \dot{q} + \omega_0^2 q - \frac{2BA}{\mu L} \int_0^L \frac{\partial^2 u(z, t)}{\partial t^2} dz \\ + \left(\frac{2B}{L_0} - \frac{2BA}{\mu L} \cdot \frac{\Delta_r}{L_0} \right) \int_0^L \frac{\partial u(z, t)}{\partial t} dz - \frac{K \hbar C_j}{2e L_0} \ddot{\varphi}(t) \\ - \frac{K \hbar}{2e L_0 C_j} \dot{\varphi}(t) - \frac{K I_c}{L_0} \sin \varphi(t) = 0. \end{aligned} \quad (7)$$

2.2 Equation of mechanical part

According to the differential equation of the dynamics of micro-beams [10,13,21], we have

$$E \cdot I_y \frac{\partial^4 u(z, t)}{\partial z^4} + \rho A \frac{\partial^2 u(z, t)}{\partial t^2} + \lambda \frac{\partial u(z, t)}{\partial t} + NLT = f(t), \tag{8}$$

with

- $u(z, t)$: function characterizing transverse displacement;
- E : Young’s modulus;
- I_y : moment of inertia;
- λ : damping coefficient of the beam;
- NLT : coefficient of nonlinearity;
- $f(t)$: actuating force of the beam;
- A : cross-sectional area of the beam;
- ρ : Density of the beam assumed to be constant.

In this study, we assume $NLT = 0.1$

The actuating force $f(t)$ of the beam is a force of Lorentz (magnetic) given by:

$$f(t) = i_p \cdot B \cdot L \sin(\mathbf{B}, \mathbf{I}).$$

As $\mathbf{B} \perp \mathbf{I}$, we have $\sin(\mathbf{B}, \mathbf{I}) = 1$, we obtain:

$$f(t) = B \times L \times i_p = B \times L \times \left(\frac{dq}{dt} + \frac{e}{r_b} \right).$$

Then

$$E \cdot I_y \frac{\partial^4 u(z, t)}{\partial z^4} + \rho A \frac{\partial^2 u(z, t)}{\partial t^2} + \lambda \frac{\partial u(z, t)}{\partial t} = B \times L \times \left[\frac{dq}{dt} - \frac{2BA}{\mu L} \int_0^L \frac{\partial u(z, t)}{\partial t} dz \right] \tag{9}$$

2.3 Equations of the dynamical system

The equations that govern the electrodynamic behavior of the sensor are written as follow:

$$\left\{ \begin{array}{l} \frac{\hbar C_j}{2e} \ddot{\varphi}(t) + \frac{\hbar}{2e} \left(\frac{K-R_j}{R_j K} \right) \dot{\varphi}(t) + I_c \sin \varphi(t) + \dot{q} \\ - \frac{2BA}{\mu L} \int_0^L \frac{\partial u(z, t)}{\partial t} dz = 0, \\ \ddot{q}(t) + \frac{\Delta_r}{L_0} \dot{q}(t) + \omega_0^2 q(t) - \frac{2BA}{\mu L} \int_0^L \frac{\partial^2 u(z, t)}{\partial t^2} dz \\ + \left(\frac{2B}{L_0} - \frac{2BA}{\mu L} \cdot \frac{\Delta_r}{L_0} \right) \int_0^L \frac{\partial u(z, t)}{\partial t} dz - \frac{K \hbar C_j}{2e L_0} \ddot{\varphi}(t) \\ - \frac{K \hbar}{2e L_0 R_j} \dot{\varphi}(t) - \frac{K I_c}{L_0} \sin \varphi(t) = 0, \\ E \cdot I_y \frac{\partial^4 u(z, t)}{\partial z^4} + \rho A \frac{\partial^2 u(z, t)}{\partial t^2} + \lambda \frac{\partial u(z, t)}{\partial t} \\ = B \times L \times \left[\frac{dq}{dt} - \frac{2BA}{\mu L} \int_0^L \frac{\partial u(z, t)}{\partial t} dz \right], \end{array} \right. \tag{10}$$

with (see [22–24]) $A = l \times w$, $\lambda = \frac{\omega_b \times m_{eff}}{Q}$

$$\omega_b = 2 \times \pi \frac{w}{L^2} \times \sqrt{\frac{E}{\rho}}$$

$$K_{eff} = 32 \times E \times l \times \frac{w^3}{L^3}; \quad m_{eff} = \frac{K_{eff}}{\omega_b^2}$$

The shape of the modes must satisfy the geometries differential and boundary conditions [21]. The deflection $u(z, t)$ of the beam can then be written as follows:

$$u(z, t) = \sum_{n=1}^{\infty} Z_n(z) T_n(t)$$

where n indicates the mode of vibration; $T_n(t)$ represents the generalized coordinate of the amplitudes and $Z_n(z)$ the set eigenfunctions of the equation:

$$\frac{\partial^4 u(z, t)}{\partial z^4} + \frac{\rho A}{E \cdot I_y} \frac{\partial^2 u(z, t)}{\partial t^2} = 0.$$

In our case we have $u(0, t) = u(L, t) = 0$ and the set eigenfunctions $Z_n(z)$ is written

$$Z_n(z) = a_n(\cos \xi_n z - \cosh \xi_n z) + b_n(\sin \xi_n z - \sinh \xi_n z),$$

where ξ_n the solution of the transcendental equation

$$\cos \xi_n L \cosh \xi_n L - 1 = 0.$$

As we focus on the study of the ground state, we take for the remain $n = 1$. By doing the standardization below

$$\int_0^L Z_1(z) Z_n(z) dz = L^3 \delta_{1,n} = \begin{cases} L^3 & \text{if } (n = 1) \\ 0 & \text{if not} \end{cases}$$

$$\text{and let's } \eta_1 = \frac{1}{L^2} \int_0^L Z_1(z) dz,$$

the system (10) gives

$$\left\{ \begin{array}{l} \ddot{\varphi}(t) + a \dot{\varphi}(t) + \omega_j^2 \sin \varphi(t) + b \dot{q} - c \dot{T} = 0 \\ \ddot{T}(t) + f \dot{T}(t) + g T(t) - h \dot{q}(t) = 0 \\ \ddot{q}(t) + \frac{\Delta_r}{L_0} \dot{q}(t) + \omega_0^2 q(t) - l_1 \ddot{T}(t) + l_2 \dot{T}(t) \\ - l_3 \ddot{\varphi}(t) - l_4 \dot{\varphi}(t) - l_5 \sin \varphi(t) = 0, \end{array} \right. \tag{11}$$

with

$$a = \left(\frac{K - R_j}{R_j K C_j} \right); \quad \omega_j^2 = \frac{2e I_c}{\hbar C_j}; \quad b = \frac{2e}{\hbar C_j};$$

$$c = \frac{4e B A \eta_1 L}{\mu \hbar C_j}; \quad f = \left(\frac{\lambda}{\rho A} + \frac{2B^2 \eta_1^2 L}{\mu \rho} \right); \quad g = \frac{E I_y \xi_1^4 \eta_1}{\rho A L};$$

$$\begin{aligned}
 h &= \frac{B \eta_1}{\rho A}; \quad l_1 = \frac{2 B A \eta_1 L}{\mu}; \quad l_3 = \frac{K \hbar C_j}{2 e L_0}; \\
 l_2 &= \left(\frac{2 B}{L_0} - \frac{2 B A}{\mu L} \times \frac{\Delta_r}{L_0} \right) \eta_1 L^2; \\
 l_4 &= \frac{K \hbar}{2 e L_0 R_j}; \quad l_5 = \frac{K I_c}{L_0}.
 \end{aligned}$$

When the micro-beam is excited at a frequency ω equals to its resonant frequency ($\omega = \omega_b$), Z_1 gives $Z_1 = \frac{f(t) \times Q}{K_{eff}}$ (see [23,24]). Considering I_0 as the maximal amplitude of the current in $f(t)$, with the above normalisation, one obtains:

$$\eta_1 = \frac{B \times I_0 \times Q}{k e f f}.$$

One of the main objectives of this study is achieved. Indeed, the coefficient of dissipation of the energy ($\frac{\Delta_r}{L_0}$) and the damping coefficient of the difference phase of the Josephson junction ($a = \frac{K - R_j}{R_j K C_j}$) depend on K which can be adjusted from the rheostat R_0 . All the dynamics of this MEMS can then be controlled from a single rheostat. The remain of this work will give more details.

After simplification, the system (11), becomes

$$\begin{cases}
 \ddot{\varphi}(t) + a \dot{\varphi}(t) + \omega_j^2 \sin \varphi(t) + b \dot{q} - c \dot{T} = 0 \\
 \ddot{T}(t) + f \dot{T}(t) + g T(t) - h \dot{q}(t) = 0 \\
 \ddot{q}(t) + \mathfrak{M}_1 \dot{q}(t) + \omega_0^2 q(t) + \mathfrak{M}_2 \dot{T}(t) + \mathfrak{M}_3 T(t) \\
 + \mathfrak{M}_4 \dot{\varphi}(t) + \mathfrak{M}_5 \sin \varphi(t) = 0,
 \end{cases} \quad (12)$$

with

$$\begin{aligned}
 \mathfrak{M}_1 &= \left(\frac{\Delta_r}{L_0} + b l_3 - h l_1 \right); \quad \mathfrak{M}_2 = (l_2 - l_3 c + l_1 f); \\
 \mathfrak{M}_3 &= l_1 g; \quad \mathfrak{M}_4 = (a l_3 - l_4); \quad \mathfrak{M}_5 = (\omega_j^2 l_3 - l_5)
 \end{aligned}$$

Using the dimensionless variables

$$\tau = \omega_1 t; \quad \beta = \frac{\varphi}{\varphi_0}; \quad \alpha = \frac{T}{T_0}; \quad \gamma = \frac{q}{Q_0},$$

we obtain

$$\begin{cases}
 \ddot{\beta}(\tau) + J_1 \dot{\beta}(\tau) + J_2 \sin [\varphi_0 \beta(\tau)] + J_3 \dot{\gamma}(\tau) - J_4 \dot{\alpha}(\tau) = 0 \\
 \ddot{\alpha}(\tau) + \sigma_1 \dot{\alpha}(\tau) + \sigma_2 \alpha(\tau) - \sigma_3 \dot{\gamma}(\tau) = 0 \\
 \ddot{\gamma}(\tau) + \varepsilon_1 \dot{\gamma}(\tau) + \varepsilon_2 \gamma(\tau) + \varepsilon_3 \dot{\alpha}(\tau) + \varepsilon_4 \alpha(\tau) + \varepsilon_5 \dot{\beta}(\tau) \\
 + \varepsilon_6 \sin [\varphi_0 \beta(\tau)] = 0,
 \end{cases} \quad (13)$$

with

$$J_1 = \frac{a}{\omega_1}; \quad J_2 = \frac{\omega_j^2}{\omega_1^2 \varphi_0}; \quad J_3 = \frac{b Q_0}{\omega_1 \varphi_0}; \quad J_4 = \frac{c T_0}{\omega_1 \varphi_0};$$

$$\begin{aligned}
 \sigma_1 &= \frac{f}{\omega_1}; \quad \sigma_2 = \frac{g}{\omega_1^2}; \quad \sigma_3 = \frac{h Q_0}{\omega_1 T_0}; \\
 \varepsilon_1 &= \frac{\mathfrak{M}_1}{\omega_1}; \quad \varepsilon_2 = \frac{\omega_0^2}{\omega_1^2}; \quad \varepsilon_3 = \frac{\mathfrak{M}_2}{\omega_1 Q_0}; \quad \varepsilon_4 = \frac{\mathfrak{M}_3 T_0}{\omega_1^2 Q_0}; \\
 \varepsilon_5 &= \frac{\mathfrak{M}_4 \varphi_0}{\omega_1 Q_0}; \quad \varepsilon_6 = \frac{\mathfrak{M}_5}{\omega_1^2 Q_0}.
 \end{aligned}$$

3 Fixed points and stability

3.1 Equilibrium points

By setting $\dot{\alpha} = x$, $y = \dot{\beta}$ and $\dot{\gamma} = z$, Eq. (13) gives:

$$\begin{cases}
 \dot{\alpha} = x \\
 \dot{x} = -\sigma_1 x - \sigma_2 \alpha + \sigma_3 z \\
 \dot{\beta} = y \\
 \dot{y} = -J_1 y - J_2 \sin [\varphi_0 \beta] - J_3 z + J_4 x \\
 \dot{\gamma} = z \\
 \dot{z} = -\varepsilon_1 z - \varepsilon_2 \gamma - \varepsilon_3 x - \varepsilon_4 \alpha - \varepsilon_5 y \\
 - \varepsilon_6 \sin [\varphi_0 \beta].
 \end{cases} \quad (14)$$

The fixed points of the MEMS are found and we note that the origin point is a fixed point and that the dynamic system possesses an infinite number of equilibrium points given by

$$E^*(\alpha^*, \dot{\alpha}^*, \beta^*, \dot{\beta}^*, \gamma^*, \dot{\gamma}^*) = E \left(0, 0, \frac{k\pi}{\varphi_0}, 0, 0, 0 \right),$$

with k is a relative integer.

3.2 Stability of the fixed points

At the fixed point E , the Jacobian is:

$$J(E^*) = \begin{bmatrix}
 0 & 1 & 0 & 0 & 0 & 0 \\
 -\sigma_2 & -\sigma_1 & 0 & 0 & 0 & \sigma_3 \\
 0 & 0 & 0 & 1 & 0 & 0 \\
 0 & J_4 & -J_2 \varphi_0 \cos [k\pi] & -J_1 & 0 & -J_3 \\
 0 & 0 & 0 & 0 & 0 & 1 \\
 -\varepsilon_4 & -\varepsilon_3 & -\varepsilon_6 \varphi_0 \cos [k\pi] & -\varepsilon_5 & -\varepsilon_2 & -\varepsilon_1
 \end{bmatrix},$$

and eigenvalues κ is given by

$$\kappa^6 + \mu_6 \kappa^5 + \mu_5 \kappa^4 + \mu_4 \kappa^3 + \mu_3 \kappa^2 + \mu_2 \kappa + \mu_1 = 0, \quad (15)$$

with

$$\begin{aligned}
 \mu_1 &= \varepsilon_2 \sigma_2 J_2 \varphi_0 \cos(k\pi) \\
 \mu_2 &= \sigma_2 J_1 \varepsilon_2 + (\sigma_2 \varepsilon_1 J_2 + \sigma_1 \varepsilon_2 J_2 - \sigma_2 \varepsilon_6 J_3)
 \end{aligned}$$

$$\begin{aligned}
 & + \sigma_3 \varepsilon_4 J_2) \varphi_0 \cos(k\pi) \\
 \mu_3 & = \sigma_2 \varepsilon_1 J_1 + \sigma_1 \varepsilon_1 J_1 + \sigma_2 \varepsilon_2 - \sigma_2 \varepsilon_5 J_3 + \sigma_3 J_1 \varepsilon_4 \\
 & + (\sigma_1 \varepsilon_1 J_2 + \varepsilon_2 J_2 - \sigma_1 \varepsilon_6 J_3 + \sigma_3 \varepsilon_6 J_4 \\
 & + \sigma_3 \varepsilon_3 J_2 + \sigma_2 J_2) \varphi_0 \cos(k\pi) \\
 \mu_4 & = \sigma_1 \varepsilon_1 J_1 + \sigma_2 \varepsilon_1 + \varepsilon_2 J_1 + \sigma_1 \varepsilon_2 - \sigma_1 \varepsilon_5 J_3 \\
 & + \sigma_3 \varepsilon_5 J_4 + \sigma_3 \varepsilon_3 J_1 \\
 & + \sigma_3 \varepsilon_4 + \sigma_2 J_1 + (\varepsilon_1 J_2 - \varepsilon_6 J_3 + \sigma_1 J_2) \varphi_0 \cos(k\pi) \\
 \mu_5 & = \varepsilon_1 J_1 + \sigma_1 \varepsilon_1 + \varepsilon_2 - J_3 \varepsilon_5 + \sigma_3 \varepsilon_3 + \sigma_1 J_1 \\
 & + J_2 \varphi_0 \cos(k\pi) + \sigma_2 \\
 \mu_6 & = \varepsilon_1 + J_1 + \sigma_1.
 \end{aligned}$$

The fixed point is stable if the eigenvalues κ are strictly negative reals or complex numbers with negative real parts or if all the determinants of Routh–Hurwitz whose expressions are defined below are all positive [14].

$$\begin{aligned}
 R_{th1} & = \mu_6 \\
 R_{th2} & = \mu_6 \mu_5 - \mu_4 \\
 R_{th3} & = -\mu_4^2 + \mu_2 \mu_6 + \mu_4 \mu_5 \mu_6 - \mu_3 \mu_6^2 \\
 R_{th4} & = -\mu_2^2 - \mu_3 \mu_4^2 + \mu_2 \mu_4 \mu_5 + 2\mu_2 \mu_3 \mu_6 - \mu_1 \mu_4 \mu_6 \\
 & + \mu_3 \mu_4 \mu_5 \mu_6 - \mu_2 \mu_6 \mu_5^2 - (\mu_3 \mu_6)^2 + \mu_1 \mu_5 \mu_6^2 \\
 R_{th5} & = -\mu_2^3 - \mu_2 \mu_3 \mu_4^2 + \mu_1 \mu_4^3 + \mu_4 \mu_5 \mu_2^2 + 2\mu_3 \mu_6 \mu_2^2 \\
 & - 3\mu_1 \mu_2 \mu_4 \mu_6 + \mu_2 \mu_3 \mu_4 \mu_5 \mu_6 - \mu_1 \mu_4^2 \mu_5 \mu_6 \\
 & - (\mu_2 \mu_5)^2 \mu_6 \\
 & - \mu_2 (\mu_3 \mu_6)^2 + \mu_1 \mu_3 \mu_4 \mu_6^2 \\
 & + 2\mu_1 \mu_2 \mu_5 \mu_6^2 - \mu_1^2 \mu_6^3 \\
 R_{th6} & = [-\mu_2^3 - \mu_2 \mu_3 \mu_4^2 + \mu_1 \mu_4^3 + \mu_4 \mu_5 \mu_2^2 + 2\mu_3 \mu_6 \mu_2^2 \\
 & - 3\mu_1 \mu_2 \mu_4 \mu_6 + \mu_2 \mu_3 \mu_4 \mu_5 \mu_6 - \mu_1 \mu_4^2 \mu_5 \mu_6 \\
 & - (\mu_2 \mu_5)^2 \mu_6 - \mu_2 (\mu_3 \mu_6)^2 + \mu_1 \mu_3 \mu_4 \mu_6^2 \\
 & + 2\mu_1 \mu_2 \mu_5 \mu_6^2 - \mu_1^2 \mu_6^3] \mu_1 = R_{th5} \mu_1
 \end{aligned}$$

For the verification of the stability of the fixed points, we chose to consider experimental values used in the literature review for the different elements of the MEMS. These values are recorded in the Tables 1, 2 and 3.

The intensity of the magnetic field $\mathbf{B} = 4T$ (see [23]) and the dimensionless coefficients are: $Q_0 = \frac{\varepsilon}{2}$; $T_0 = 10^{-20}m$; $\varphi_0 = \frac{\pi}{3}$; $R_1 = R_2$ and $R_0 = R_j$

For the different possible values of k , we have calculated the determinants of the Routh–Hurwitz matrices for each of the two types of Josephson junctions considered. For $k = 2n + 1, n \in \mathbb{Z}$ and for both types of junctions it should be noted that the fixed points are unstable because R_{th5} is negative (see Table 4). For $k = 2n, n \in \mathbb{Z}$, all the determinants of the calculated Routh–Hurwitz matrices are positive and it can then be concluded that the fixed points are stables.

Table 1 Dimension and important parameters of the silicon micro-beam of quality factor $Q = 10^4$ at 300 K (see [23])

Beam Parameters	Values
Length (L)	$2 \cdot 10^{-6} \text{ m}$
Width (l)	$100 \cdot 10^{-9} \text{ m}$
Thickness (w)	$200 \cdot 10^{-9} \text{ m}$
Electrical resistivity (μ)	$0.2582 \ \Omega \text{ m}$
Volume density (ρ)	2330 kg m^{-3}
Young’s modulus (E)	150 GPa

All other parameters related to the micro-beam will be calculated on the basis of formulas well listed in [22] and the above values

Table 2 Values of the critical current (I_{C_j}) and the normal resistance R_j or the different types of Josephson junctions present in the literature and used for our study

Josephson junction types	$I_{C_j} (\mu\text{A})$	$R_j (\Omega)$
NCCO [25]	2.2	15
Tricritical [26]	0.114	100

NCCO/Au/In; Tricritical of LCCO For each Josephson junction, the value of the capacity C_j eis in order of pF . For the calculus, we will take $5pF$

Table 3 I_0 values (excitation current amplitude of the micro beam); capacity C_0 of the capacitor; inductance L_0 of the coil and its internal resistance r_0

Parameters	Values
I_0	$5 \ \mu\text{A}$
L_0	$50 \ \mu\text{H}$
C_0	$50 \ \text{pF}$
r_0	$5 \ \Omega$

$$E^*(\alpha^*, \dot{\alpha}^*, \beta^*, \dot{\beta}^*, \gamma^*, \dot{\gamma}^*) = E(0, 0, \frac{2n\pi}{\varphi_0}, 0, 0, 0).$$

The theoretical studies show us that the electro-dynamic behavior of the dynamic system can be controlled by the rheostat R_0 . This dynamic system has several fixed points. These equilibrium points strongly depend on the phase difference φ of the Josephson junction. Indeed, for $k = 2n + 1$, the fixed points $E^*(\alpha^*, \dot{\alpha}^*, \beta^*, \dot{\beta}^*, \gamma^*, \dot{\gamma}^*) = E(0, 0, \frac{(2n+1)\pi}{\varphi_0}, 0, 0, 0)$ are unstables and for $k = 2n$, the fixed points $E^*(\alpha^*, \dot{\alpha}^*, \beta^*, \dot{\beta}^*, \gamma^*, \dot{\gamma}^*) = E(0, 0, \frac{2n\pi}{\varphi_0}, 0, 0, 0)$ are stables.

4 Numerical study

We begin this section by illustrating the electro-dynamic behavior of the MEMS for the experimental values of the constitutive elements of the selected MEMS. Table 5 illustrates the values of the control parameters of the system computed

Table 4 Value of the determinants of the Routh–Hurwitz matrices for each type of Josephson junction for $Q_0 = \frac{e}{2}$; $T_0 = 10^{-20}m$; $\varphi_0 = \frac{\pi}{3}$

Type of Josephson junction and value of k	Value of R_{th_i}
NCCO/Au/In for $k = 2n$	13.827659759192157
	$9.9469709025079567 \times 10^{-3}$
	0.14326651339655427
	$4.4920838604411983 \times 10^{-7}$
	$1.2571035767905414 \times 10^{-8}$
	$3.9355671499485823 \times 10^{-14}$
Tricristal of LCCO for $k = 2n$	60.744587588248464
	0.84326894812943465
	1025.7682792436099
	2.2754272720776498
	1324.4285297393799
	1.5438407058827579
NCCO/Au/In for $k = 2n + 1$	13.827659759192157
	$9.9469709025123976 \times 10^{-3}$
	0.14212239628994894
	$2.1569028945123137 \times 10^{-6}$
	$-2.4715825475141173 \times 10^{-5}$
	$7.7359471259419443 \times 10^{-11}$
Tricristal of LCCO for $k = 2n + 1$	60.744587588248464
	0.84326894812966202
	1025.3421845840203
	2.5122808555606753
	-1614.8980779647827
	1.8824310447089374

according to each type of Josephson junction with the initial conditions defined as:

$$\begin{aligned} \gamma(0) &= \frac{1.60217656 \cdot 10^{-19}}{2}; & \dot{\gamma}(0) &= 0; \\ \alpha(0) &= 10^{-20}; & \dot{\alpha}(0) &= 0; & \dot{\beta}(0) &= 0; \\ \beta(0) &= \frac{3.141592653589793}{3}; & B &= 4T. \end{aligned}$$

To simplify the analyzes according to the rheostat setting, we will take $R_1 = R_2$ and the normalize time as $\frac{1}{\omega_j}$ ie $\omega_1 = \omega_j$ (see [27]).

In a first step, we analyzed the stability of the fixed points studied in the analytical part of our work with the same experimental values taken from the literature. Secondly, we have illustrated a few different techniques for controlling the electro-dynamic modes of the micro-system through the influence of the Josephson junction on the system by adjustment of the rheostat. Tertio, an explanation of the name ‘‘Active Sensor’’ is given with the different plausible abilities of this

Table 5 Calculus of control parameter values for $R_0 = K = R_j$ for each Josephson junction

Types of Josephson junction	Values of control parameters
NCCO/Au/In	$J_1 = 0.0000000000000000$
	$J_2 = 0.95492963197803404$
	$J_3 = 1.2714156032474 \times 10^{-3}$
	$J_4 = 8.3708357073384 \times 10^{-26}$
	$\varepsilon_1 = 13.8276597591815$
	$\varepsilon_2 = 2.9918727198979 \times 10^{-6}$
	$\varepsilon_3 = 9.1039452296069 \times 10^{-2}$
	$\varepsilon_4 = 6.8877363696306 \times 10^{-23}$
	$\varepsilon_5 = -2.3531823207581 \times 10^{-3}$
	$\varepsilon_6 = 0.0000000000000000$
	$\sigma_1 = 1.0643636599981 \times 10^{-11}$
	$\sigma_2 = 1.04615307211515$
	$\sigma_3 = 7.8358256789718 \times 10^{-3}$
Tricristal of LCCO	$J_1 = 0.0000000000000000$
	$J_2 = 0.95492963197803415$
	$J_3 = 5.5852991625130 \times 10^{-3}$
	$J_4 = 3.6772886494638 \times 10^{-25}$
	$\varepsilon_1 = 60.744587588201711$
	$\varepsilon_2 = 5.7737891480006 \times 10^{-5}$
	$\varepsilon_3 = 0.399932850967665$
	$\varepsilon_4 = 1.3292122101577 \times 10^{-21}$
	$\varepsilon_5 = -1.0337475182623 \times 10^{-2}$
	$\varepsilon_6 = 1.0002320396609 \times 10^{-17}$
	$\sigma_1 = 4.6757247933820 \times 10^{-11}$
	$\sigma_2 = 20.188917846518539$
	$\sigma_3 = 3.4422599888324 \times 10^{-2}$

MEMS. Finally, a study of the influence of some important parameters of control will be done.

4.1 Electro-dynamic behavior for $R_0 = K = R_j$

When the rheostat is reset such that $R_0 = R_j$, j_1 which is the parameter of dissipation of the phase of the Josephson junction is canceled. Thus, the phase difference losses of the junction can be corrected from the R_0 rheostat of the auxiliary generator. For each of the junctions used we have presented the phase diagrams and the times histories of the main variables of our electromechanical system in this experimental condition. The values of the control parameters in this case are recorded in the Table 5 for each type of Josephson junction. We have chosen to present this table with the values of the control parameters calculated at a high order, given the very high sensitivity of the electrodynamic modes to the slightest variation of these parameters. Figures 2 and 3 illustrate the electrodynamic behaviors respectively for the types junctions NCCO/Au/In and Tricristal of LCCO.

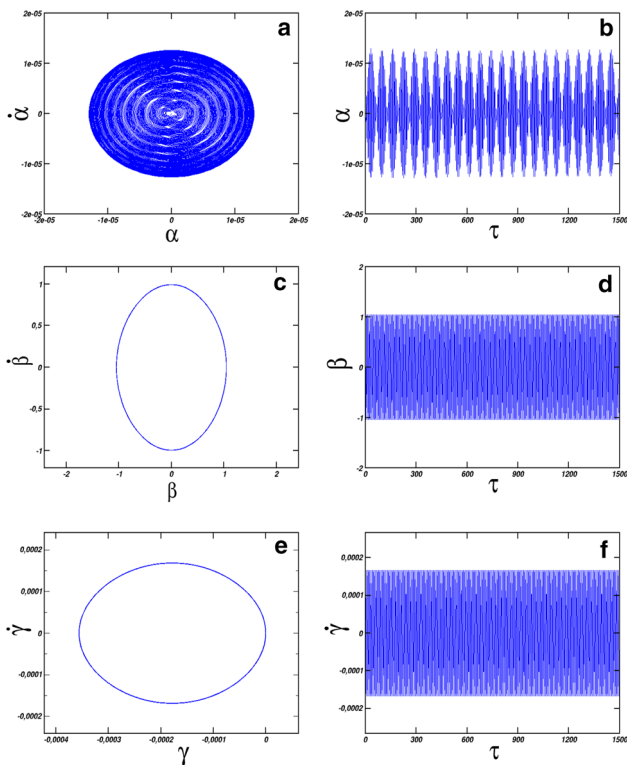


Fig. 2 Electrodynamic behavior of the system with $R_0 = R_j = 15\Omega$ for the junction NCCO/Au/In **a** phase space of the flexural vibration of the micro-beam; **b** time histories of the oscillations of the micro-beam; **c** phase space of the phase difference of the Josephson junction **d** times histories of the phase difference of Josephson junction; **e** phase space of the electric charge of the capacitor C_0 ; **f** times histories of the charge current of the capacitor C_0

From Figs. 2 and 3 we note as expected by the analytical calculations that for $J_1 = 0$, the oscillations of the phase difference of the Josephson junctions are periodic and harmonic (see Figs. 2, 3c, d). The micro-beam presents a quasi-periodic oscillation well justified by the graphs of the phase spaces and those of the Poincaré section (Figs. 4, 5) for each type of junction. We also note that the vibration amplitudes differ from one junction to another. In fact, for the MEMS with the NCCO/Au/In type junction, the maximum amplitudes of the micro-beam reach tens of times those of the MEMS with the type junction tricristal of LCCO (see Figs. 2, 3a, b). One could therefore model the amplitudes and even the oscillation frequencies of the micro-beam of this MEMS by an efficient choice of the type of Josephson junction used. We also note a similarity between the phase difference dynamics of the Josephson junction and that of the electric resonator (r_0, L_0, C_0) (see Figs. 2, 3e, f).

4.2 Electrodynamic behavior with $R_0 = K < R_j$

In order to deepen the analysis of the influence of the Josephson junction on the system using a simple rheostat, we have studied each of the cases where the parameter $J_1 < 0$ and

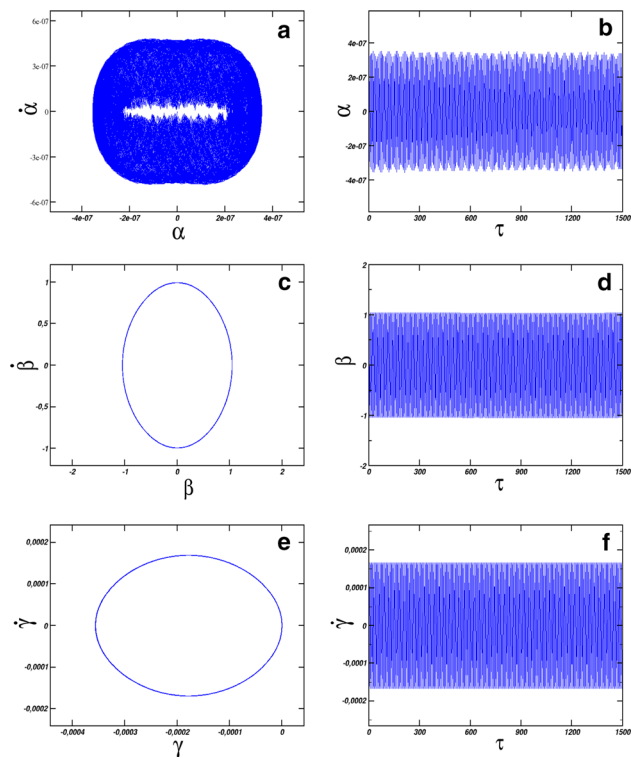


Fig. 3 Electrodynamic behavior of the system with $R_0 = R_j = 100\Omega$ for the junction Tricristal of LCCO **a** phase space of the flexural vibration of the micro-beam; **b** time histories of the oscillations of the micro-beam; **c** phase space of the phase difference of the Josephson junction **d** times histories of the phase difference of Josephson junction; **e** phase space of the electric charge of the capacitor C_0 ; **f** times histories of the charge current of the capacitor C_0

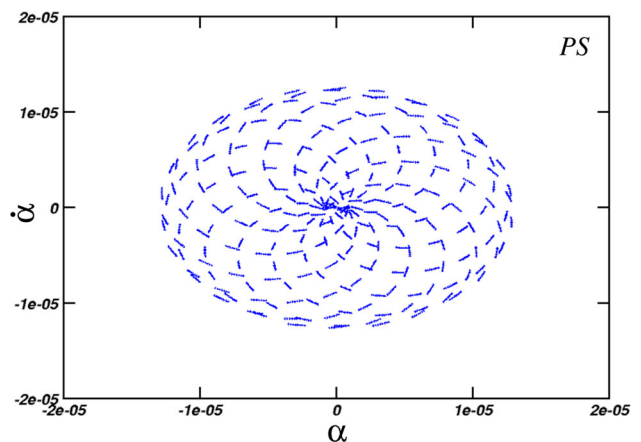


Fig. 4 Poincaré section of the micro beam for $R_0 = R_j = 15\Omega$ with the junction NCCO/Au/In

$J_1 > 0$. Indeed, for $J_1 < 0$, one has $K = R_0 < R_j$ in this case, amplitudes are amplified not only at the phase difference of the Josephson junction but also at the level of the electrical and mechanical oscillations. Figures 6 and 7 illustrate this gain in the electrical and mechanical energy of the system. The graphs (d) and (g) of Figs. 6 and 7 illustrate once again the similarity between the oscillatory behavior of

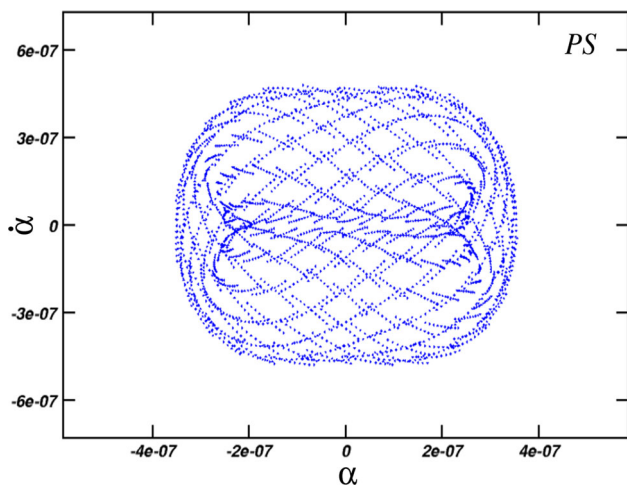


Fig. 5 Poincaré section of the micro beam for $R_0 = R_j = 100\Omega$ with the junction Tricristal of LCCO

the phase difference of the junction and that of the capacitor charge C_0 . We can therefore conclude that the oscillatory behaviors of the Josephson junction can be visualized on the screen of an oscilloscope just by visualizing the voltage across the capacitor C_0 . In fact, this is justified by the fact that the phase difference φ of the Josephson junction and the charge q of the capacitor C_0 present almost the same paces on their times histories. Knowing that $u_{c_0}(t) = \frac{1}{C_0} \times q(t)$, one could thus visualize the modes of oscillations of the phase difference of the junction through the shape of the voltage at the terminals of C_0 . The energy gains can be used in several areas such as the electric charges of charge micro-capacitors, and delay actuators. Indeed, the excesses of the charging current could be recovered by micro-capacitors and used to supply other micro-systems with energy deficiency. Increasing the oscillation amplitudes of the micro-beam could serve as a high-precision time delay mechanical actuator. Also, the indefinite evolution of this system over time could lead to the breakdown of the C_0 capacitor with spark emission. This phenomenon can be used in the field of military security to trigger explosions of fuel bombs.

Aside from these interesting characteristics above the number, the MEMS for some of these values of $J_1 < 0$ (ie $R_0 < R_j$) presents an interesting and very interesting feature in the field of information security. Indeed, on Figs. 6 and 7 we observe phase diagrams with random paces and times histories with chaotic oscillations. Poincaré section of Figs. 8 and 9 confirm the irregularities and oscillatory imprecision of the micro-beam for this value of R_0 .

4.3 Electrodynamic behavior with $R_0 = K > R_j$

When $R_0 = K > R_j$, we observe a damping of oscillatory amplitudes at all levels. Although this dynamic does not present too much physical interest for this MEMS at this

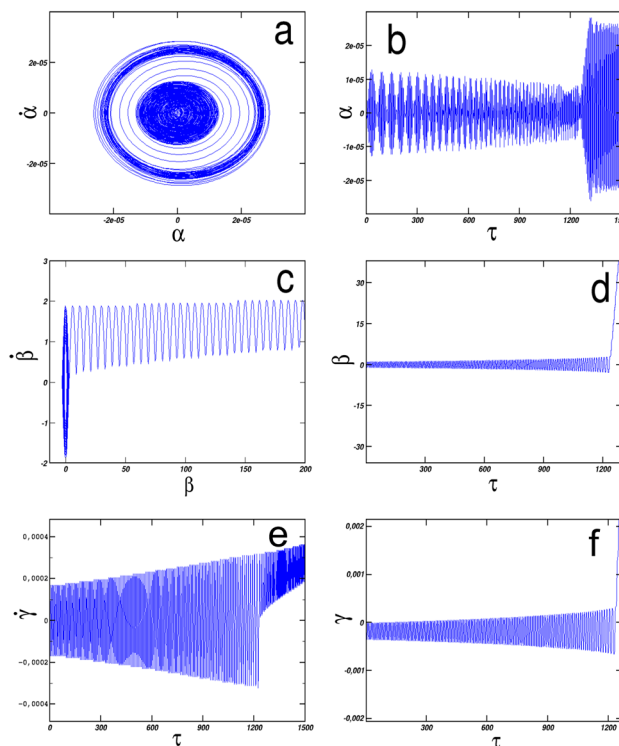


Fig. 6 Electrodynamic behavior with $R_0 = 14.95\Omega < R_j$ for the junction NCCO/Au/In **a** phase space of the flexural vibration of the micro-beam; **b** time histories of the oscillations of the micro-beam; **c** phase space of the phase difference of the Josephson junction **d** times histories of the phase difference of Josephson junction; **e** times histories of the charge current of the capacitor C_0 ; **f** times histories of the charge of the capacitor C_0 . $J_1 = -1.219 \times 10^{-3}$; $J_2 = 0.955$; $J_3 = 1.271 \times 10^{-3}$; $J_4 = 8.371 \times 10^{-26}$; $\epsilon_1 = 13.827$; $\epsilon_2 = 2.992 \times 10^{-6}$; $\epsilon_3 = 9.104 \times 10^{-2}$; $\epsilon_4 = 6.888 \times 10^{-23}$; $\epsilon_5 = -2.353 \times 10^{-3}$; $\epsilon_6 = -1.0366 \times 10^{-18}$; $\sigma_1 = 1.064 \times 10^{-11}$; $\sigma_2 = 1.046$; $\sigma_3 = 7.836 \times 10^{-3}$.

time, we have chosen to illustrate the concordance between analytic studies and numerical simulations with real experimental quantities. Figures 10 and 11 illustrate this negative loss for NCCO/Au/In junction only.

From all of the foregoing, we can come to the conclusion that electrodynamic modes of the ds MEMS strongly depend on the mode of variation of the Josephson junction phase difference. Indeed as in [28] the graphs above show that the Josephson junction has a great influence on the dynamics of the MEMS and that all the electrodynamic modes going through the chaotic regimes could be obtained just by a simple adjustment of the rheostat R_0

4.4 Practical interests of this MEMS

4.4.1 Measuring of the normal resistance of a Josephson junction

As previously stated and as already illustrated by Figs. 3, 6, 7, 10 and 11, a small variation in the value of the rheostat in the

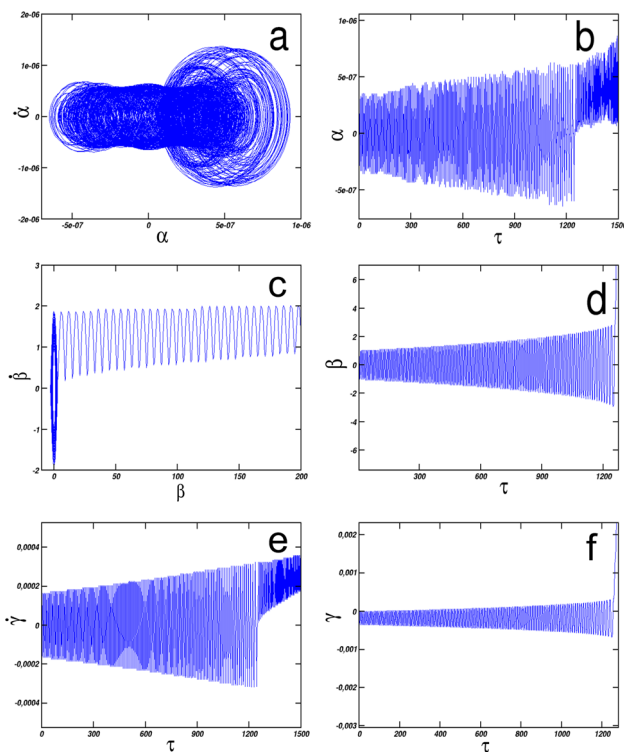


Fig. 7 Electrodynamic behavior with $R_0 = 99.5\Omega < R_j$ for the junction Tricristal of LCCO **a** phase space of the flexural vibration of the micro-beam; **b** time histories of the oscillations of the micro-beam; **c** phase space of the phase difference of the Josephson junction **d** times histories of the phase difference of Josephson junction; **e** times histories of the charge current of the capacitor C_0 ; **f** times histories of the charge of the capacitor C_0 . $J_1 = -1.207 \times 10^{-3}$; $J_2 = 0.955$; $J_3 = 5.585 \times 10^{-3}$; $J_4 = 3.677 \times 10^{-25}$; $\varepsilon_1 = 60.744$; $\varepsilon_2 = 5.774 \times 10^{-5}$; $\varepsilon_3 = 0.399$; $\varepsilon_4 = 1.329 \times 10^{-21}$; $\varepsilon_5 = -1.0337 \times 10^{-2}$; $\varepsilon_6 = 5.001 \times 10^{-18}$; $\sigma_1 = 4.6757 \times 10^{-11}$; $\sigma_2 = 20.1889$; $\sigma_3 = 3.442 \times 10^{-2}$

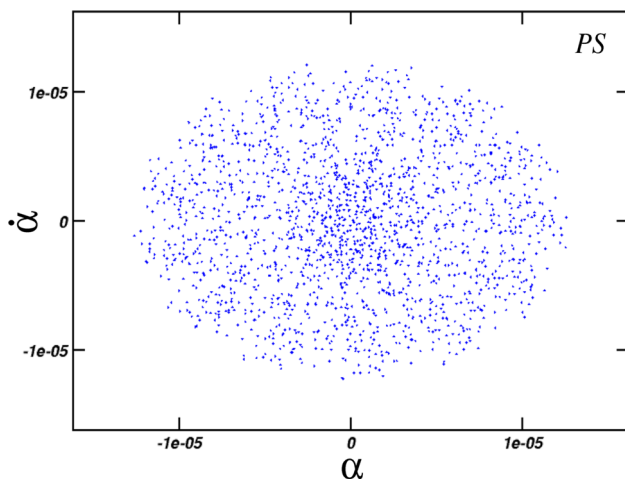


Fig. 8 Poincaré section of the micro beam for $R_0 = R_j = 14.95\Omega$ with junction NCCO/Au/In

vicinity of the value of the normal resistance R_j of the Josephson junction induces remarkable effects on the type of both mechanical and electrical oscillation of the MEMS. Indeed,

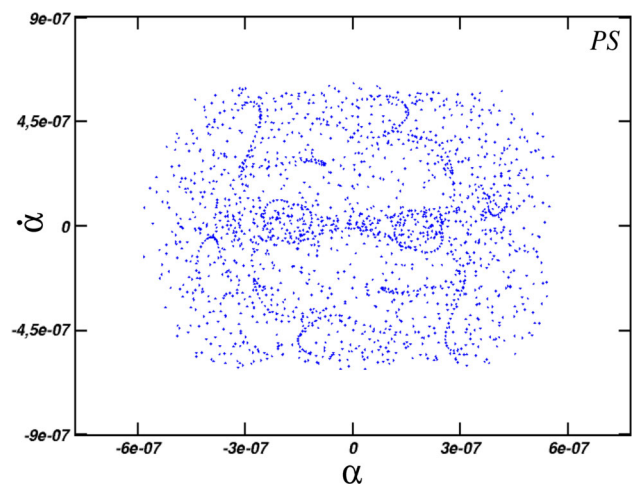


Fig. 9 Poincaré section of the micro beam with $R_0 = 99.5\Omega < R_j$ for the junction Tricristal of LCCO

we have already mounted how most of the dynamic modes can be visualized through the voltage across the capacitor C_0 . Thus, when the rheostat would be set to the approximate value of R_j , the voltage across the capacitor C_0 would present harmonic and periodic oscillations as shown in the graphs (f) of Figs. 2 and 3. As an example, we have chosen to show an example for a variation ($\Delta R_0 = -0.1$) with the Tricristal of LCCO junction. Figure 11 shows the difference between the periodic mode obtained for $R_0 = R_j = 100\Omega$ (see Fig. 3) and that obtained for $R_0 = 99.9$.

We see that for this small variation of ΔR_0 in the neighborhood of R_j , the periodic and harmonic oscillations of Fig. 3 are lost at all levels

4.4.2 Influence of the temperature of the micro-beam on the mechanical and electrical oscillations of the system

We have evaluated the influence of the temperature on the mechanical and electrical oscillations of the system since the control temperature is a very important factor in several fields such as chemistry, aeronautics, agro-food industries, storage centers, air-conditioning systems and others. Indeed, the strong correlation between the temperature and the resistivity of semiconductors is well established. If, in pure semiconductors, the growth of the temperature induces the growth of the resistivity electric power, the opposite effect is observed in silicon (see [29]). To highlight this temperature-resistivity relationship, we have plotted the curves giving the maxima of the amplitude of vibration of the micro-beam and the load current of the capacitor C_0 in order to appreciate the influence of the temperature on the micro-system (see Fig. 12).

It can be seen that the maximum amplitudes of the variables of the two resonators (electrical and mechanical)

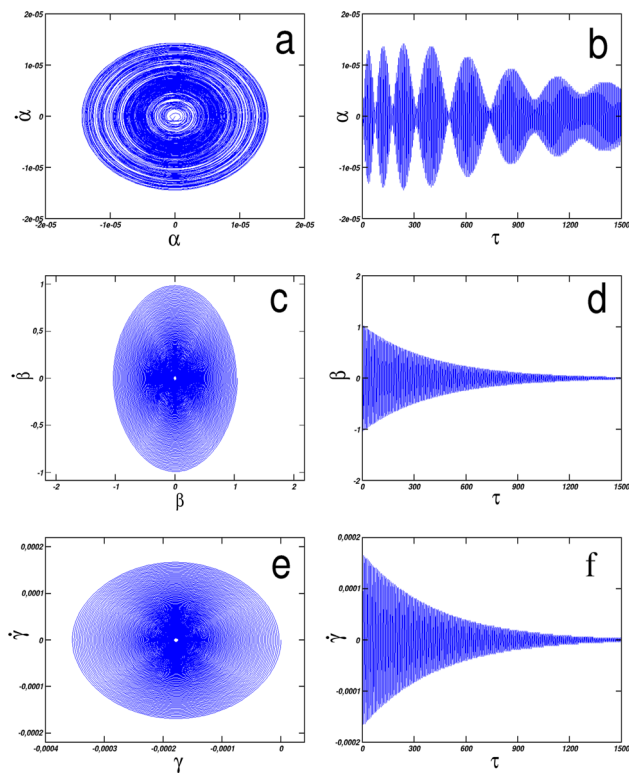


Fig. 10 Electrodynamic behavior with $R_0 = 15.2\Omega > R_j$ for the junction NCCO/Au/In **a** phase space of the flexural vibration of the micro-beam; **b** time histories of the oscillations of the micro-beam; **c** phase space of the phase difference of the Josephson junction **d** times histories of the phase difference of Josephson junction; **e** phase space of the electric charge of the capacitor C_0 ; **f** times histories of the charge current of the capacitor C_0 . $J_1 = 4.798 \times 10^{-3}$; $J_2 = 0.955$; $J_3 = 1.271 \times 10^{-3}$; $J_4 = 8.371 \times 10^{-26}$; $\varepsilon_1 = 13.827$; $\varepsilon_2 = 2.992 \times 10^{-6}$; $\varepsilon_3 = 9.104 \times 10^{-2}$; $\varepsilon_4 = 6.888 \times 10^{-23}$; $\varepsilon_5 = -2.353 \times 10^{-3}$; $\varepsilon_6 = -1.0366 \times 10^{-18}$; $\sigma_1 = 1.064 \times 10^{-11}$; $\sigma_2 = 1.046$; $\sigma_3 = 7.836 \times 10^{-3}$

increase with the decrease of the electrical resistivity. In other words, the oscillatory amplitudes decrease with the growth of the temperature. Since the micro-beam, given its physical characteristics, would be very sensitive to the variation of the temperature and this variation of the temperature induces that of its electrical resistivity, we can say that this micro-machine could serve as a good active sensor of temperature. Indeed, the physical quantity that is the temperature is captured by the micro-membrane vibrating of the micro-beam and transcribed in electrical signal which is expressed by an increase of the amplitudes of the current of load and the electric voltage at the terminals of the capacitor C_0 . This effect is accentuated when the electrical resistivity $\mu < 0.25\Omega/\text{m}$. In other words, when the temperature is less than 25°C , a small variation of the latter causes a considerable increase in the magnitude of the charging current and the electrical voltage across the capacitor C_0 . This feature could give the MEMS capabilities to serve as a temperature sensor in the field of cryogenics, aeronautics and air conditioning. The considerable load gain observed for these temperatures could

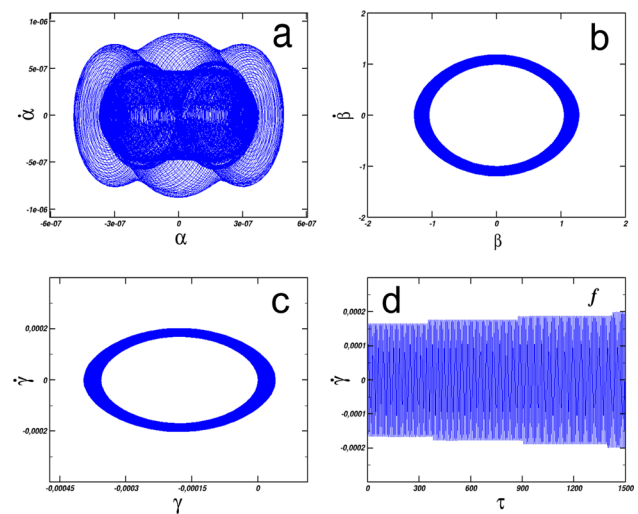


Fig. 11 Electrodynamic behavior with $R_0 = 99.9\Omega$ for the junction Tricristal LCCO **a** phase space of the flexural vibration of the micro-beam; **b** phase space of the phase difference of the Josephson junction; **c** phase space of the electric charge of the capacitor C_0 ; **d** times histories of the charge current of the capacitor C_0

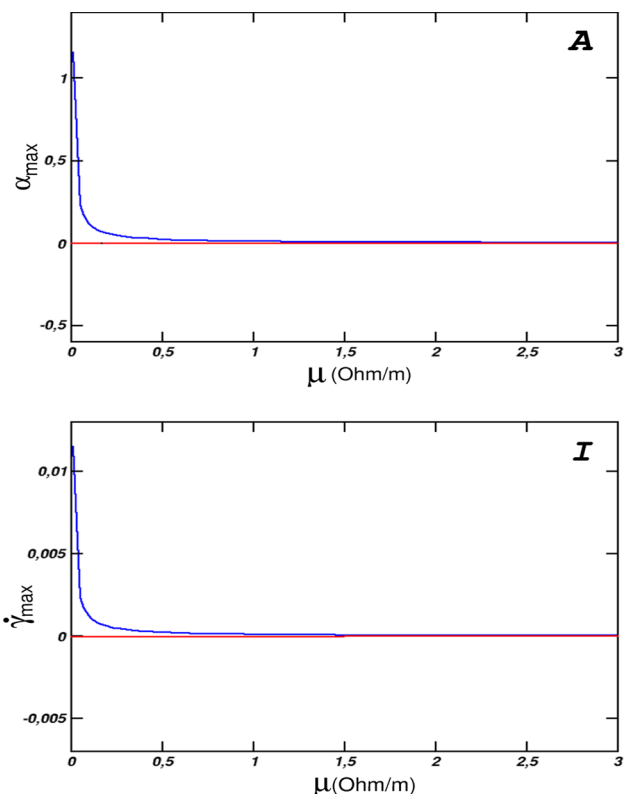


Fig. 12 Variation of the maximum amplitudes of mechanical oscillations (A) and those of electricity (I) as a function of the electrical resistivity of the silicon micro-beam for the junction NCCO/Au/In with $R_0 = R_j = 15\Omega$

also be used to charge micro-electrical systems in temperate zones. As generally mentioned in the literature, the thermal production of electricity is due to the rise in temperature,

the particularity of this MEMS would then be its capacity to increase its electricity production when the temperature drops further.

4.4.3 Influence of the magnetic field on the mechanical and electrical oscillations of the system

We are finally interested in the reaction of the MEMS in the absence of a magnetic field and also in the presence of magnetic fields weaker than that used so far. Indeed, to increase the sensitivity of the silicon membrane, we chose to reduce its electrical resistivity for these simulations. Thus, the least forces could excite considerably the vibrating membrane of the micro-beam. We then examined the electro-dynamic behavior of the MEMS for $B = 0T$; $B = 10^{-2}T$ and $B = 10^{-1}T$. Figures 13, 14 and 15 illustrate MEMS electro-dynamic behaviors for these values of B respectively.

For $B = 0T$ as expected, we see that the micro-beam has a static motion (see Fig. 13b). The membrane of the micro-beam remained in its chosen initial position for our simulations. For $B = 10^{-2}T$ there is an almost periodic oscillation of the micro-beam (see Fig. 14b) with a low frequency of vibration. The oscillation frequency of the mechanical resonator (micro-beam) is in this case much lower than that of the electric resonator (see Fig. 14b, f). For $B = 10^{-1}T$, the dynamics are qualitatively similar to the previous one but major quantitative differences are observed. The maximum amplitudes of oscillations of the micro beam go from 1.5×10^{-8} to 3.5×10^{-7} (magnitude without unit because dimensionless) and the oscillation frequency of the micro-beam is more than the triple of those obtained for

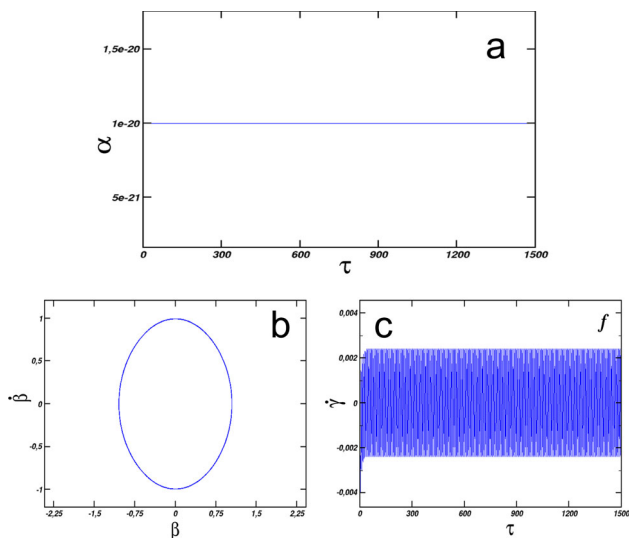


Fig. 13 Electrodynamic behavior with $\mu = 2.5 \times 10^{-3} \Omega \text{ m}$; $B = 0T$; $R_0 = 15\Omega$ for the junction NCCO/Au/In. **a** Time histories of the oscillations of the micro-beam; **b** phase space of the phase difference of the Josephson junction **c** times histories of the charge current of the capacitor C_0

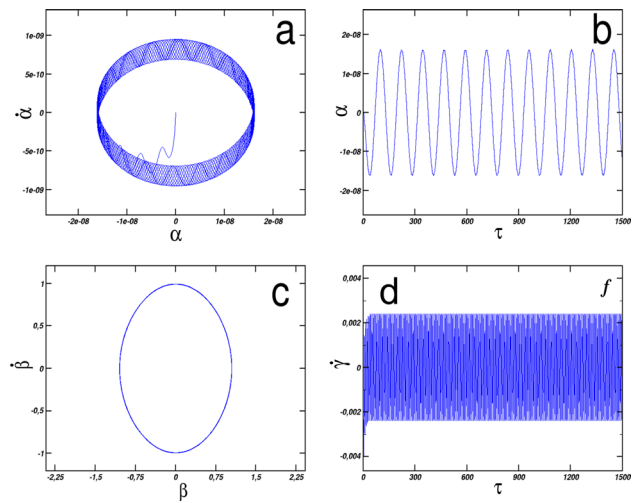


Fig. 14 Electrodynamic behavior with $\mu = 2.5 \times 10^{-3} \Omega \text{ m}$; $B = 0.01T$; $R_0 = 15\Omega$ for the junction NCCO/Au/In. **a** phase space of the flexural vibration of the micro-beam; **b** time histories of the oscillations of the micro-beam; **c** phase space of the phase difference of the Josephson junction **d** times histories of the charge current of the capacitor C_0

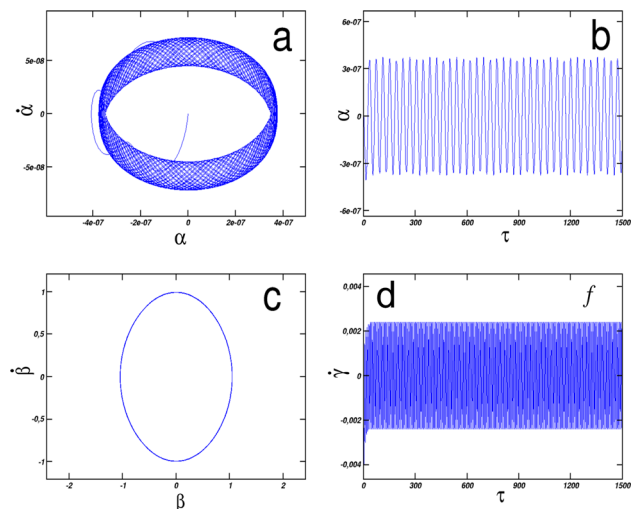


Fig. 15 Electrodynamic behavior with $\mu = 2.5 \times 10^{-2} \Omega \text{ m}$; $B = 0.1T$; $R_0 = 15\Omega$ for the junction type NCCO/Au/In. **a** phase space of the flexural vibration of the micro-beam; **b** time histories of the oscillations of the micro-beam; **c** phase space of the phase difference of the Josephson junction **d** times histories of the charge current of the capacitor C_0

$B = 10^{-2}T$; from 12 periods to 38 (see Figs. 14b, 15b). From all these observations, it can be concluded on the one hand that the mechanical part of this MEMS is very sensitive to the slightest variation of the magnetic field. We note a conversion of the variation of the magnetic field in frequency oscillation. This feature could give the MEMS the function of a magnetic field transducer. On the other hand, as shown in the Figs. 14b and 15b the two energy self-sufficient MEMS resonators can simultaneously oscillate at different frequencies. This could be a very useful property in the field

of signal processing. Indeed, since the oscillation frequency of the micro-beam can be modeled by means of a uniform magnetic field, this MEMS could offer capabilities to simultaneously process multi-frequency signals.

5 Conclusion

This study focused on a MEMS sensor essentially consisting of a Josephson junction, a microbeam, a dipole (R,L,C) and an auxiliary generator. Our goal in this work is to model an energy-efficient MEMS capable of playing the role of a temperature and/or magnetic field sensor B . Indeed, a feature of this MEMS we propose is its ability to convert low temperatures into electrical energy. The influence of the Josephson junction on the electromechanical oscillations frequencies of this MEMS has been illustrated. It is obtained that the conservation or not of the energies of this active sensor can be controlled by means of a simple rheostat of the auxiliary generator. For this dynamic system, an infinite number of fixed points is obtained. Through the phase spaces, we have shown that the dynamic behaviors of the micro-beam are strongly related to those of the Josephson junction. The chaotic behavior of one induces that of the micro-beam. The influence of each control parameter has been studied and some dynamics have been illustrated. It goes out of this study also that several chaotic regimes have been obtained.

References

- Roukes M (2001) Nanoelectromechanical systems face the future. *PhysicsWeb Phys World Mag* 14:2
- Salem FM, Sastry S (1989) The complete dynamics of the forced Josephson junction circuit: the region of chaos. *MEMO DUMEM SM* 83/02/
- Salem FM, Sastry S (1984) Summary of the complete dynamics of the forced Josephson junction circuit: the region of chaos. In: *Proc IEEE ISCAS*
- Abidi AA, Chua LO (1979) On the dynamics of Josephson junction circuit. *Electron Circuits Syst* 3(4):186–200
- Ben-Jacob E, Goldhirsch I, Imry Y, Fishman S (1982) Intermittent chaos in Josephson junctions. *Phys Rev Lett* 49:1599–1602
- Belykh VN, Pedersen NF, Soerensen OH (1977) Shunted Josephson junctions model I-the autonomous case II-the non-autonomous case. *Phys Rev B* 16(11):4853–4871
- Valkering TP, Hooijer CLA, Kroon FM (2000) Dynamics of two capacitively coupled Josephson junctions in the overdamped limit. *Phys D* 135:137–153
- James BA, Gregory BL, Smith HJT (2000) Intermittent synchronization of resistively coupled chaotic Josephson junctions. *Phys Rev B* 62(9):5931
- Nuznetsov AP, Sataev IR, Sedova YV (2018) Dynamics of three and four non-identical Josephson junctions. *J Non Appl Nonlinear Dyn* 7(1):105–110
- Domguia SU, Abobda LT, Wofo P (2015) Dynamical behavior of a capacitive microelectromechanical system powered by Hindmarsh–Rose electronic oscillator. *J Comput Nonlinear Dyn* 11(5):051006
- Yamapi R, Chabi Orou JB, Wofo P (2003) Harmonic dynamics and transition to chaos in a nonlinear electromechanical system with parametric coupling. *Phys Scr* 67(4):269
- Yamapi R, Filatrella G (2014) Noise effect on birhythmic Josephson junction coupled to a resonator. *Phys Rev E* 89:052905
- Kwuimy CAK, Wofo P (2010) Modeling and dynamics of the self-sustained electrostatic microelectromechanical system. *J Comput Nonlinear Dyn* 5(2):021010
- Nayfeh AH, Mook T (1995) *Nonlinear oscillations*. Wiley, New York
- Bartuccelli M, Gentile G, Wright JA (2016) Stable dynamics in forced systems with sufficiently high/low forcing frequency. *Chaos* 26:083108
- Enjieu KG, Nana NRB, Chabi Orou JB, Talla PK (2007) Nonlinear dynamics of plasma oscillations modeled by an anharmonic oscillator. *Phys Plasmas* 15:1–14
- Enjieu KHG, Chabi Orou JB, Wofo P (2008) Regular and chaotic behaviors of plasma oscillations modeled by a modified Duffing equation. *Phys Scr* 77:025503
- Miwadinou CH, Hinvi LA, Monwanou AV, Chabi Orou JB (2017) Nonlinear dynamics of a ϕ^6 -modified Duffing oscillator: resonant oscillations and transition to chaos. *Nonlinear Dyn* 88:97–113
- Chang TP (2017) Chaotic motion in forced Duffing system subject to linear and nonlinear damping. *Math Prob Eng* 2017:3769870
- Zebrowski JJ, Grudzinski K, Buchner T, Kuklik P, Gac J, Gielerak G, Sanders P, Baranowski R (2007) Nonlinear oscillator model reproducing various phenomena in the dynamics of the conduction system of the heart. *Chaos* 17:015121
- Geronymos S (2014) Modélisation vibratoire en flexion des poutres composites multicouches à section creuse suite à un impact. *Ecole polytechnique de Montréal, Département de mécanique, Mémoire ès sciences appliquées*
- Ekinci KL, Yang YT, Roukes ML (2004) Ultimate limits to inertial mass sensing based upon nanoelectromechanical systems. *J Appl Phys* 95:2682–2689
- Ekinci KL, Roukes ML (2005) Nanoelectromechanical systems. *Rev Sci Instrum* 76:061101
- Mohanty P, Harrington DA, Ekinci KL, Yang YT, Murphy MJ, Roukes ML (2002) Intrinsic dissipation in high-frequency micromechanical resonators. *Phys Rev B* 66:085416
- Ariando DD, Smilde HGH, Léca V, Blank DHA, Rogalla H, Hilgenkamp H (2005) Phase-sensitive order parameter symmetry test experiments utilizing $Nd_{2-x}Ce_xCuO_4/Nb$ zigzag junction. *Phys Rev Lett* 94:167001
- Chisca B, Ehrhardt K, Möhle M, Straub R, Koelle D, Kleiner R, Tsukada A (2003) Magnetic-field dependence of the maximum supercurrent of $La_{2-x}Ce_xCuO_{4-y}$ inter-ferometers: evidence for a predominant $d_{x^2-y^2}$ superconducting order parameter. *Phys Rev Lett* 90(5):057004
- James AB, Matteo C, Grøbech-Jensen N (2015) A survey of classical and quantum interpretation of experiments on Josephson junction at very low temperatures. *Phys Rep* 611(10):010
- Koudafoké GN, Miwadinou CH, Hinvi AL, Monwanou AV, Chabi Orou JB (2019) Modeling and study of dynamics of micro-beam coupled to two Josephson junctions. *Scr Phys*. <https://doi.org/10.1088/1402-4896/ab30e6>
- Cazzare A, Vehil-R Bonnet G, Morancho F, Austin P (2005) Dépendance en température des propriétés de conduction du silicium massif. *J3eA*. <https://doi.org/10.1051/j3ea:2006014>